Electrostatic depletion effects on the stability of colloidal dispersions of charged sepiolite and natural rubber latex

Irene Tagliaro,[†] Barbara Di Credico,[†] and Arturo Moncho-Jordá[*,‡,¶]

[†]*Department of Materials Science, University of Milano-Bicocca, INSTM, Via R. Cozzi, 55, 20125 Milano, Italy*

[‡]*Departamento de Física Aplicada, Facultad de Ciencias, Universidad de Granada, Campus Fuentenueva S/N, 18071 Granada, Spain.*

[¶]*Instituto Carlos I de Física Teórica y Computacional, Facultad de Ciencias, Universidad de Granada, Campus Fuentenueva S/N, 18071 Granada, Spain.*

E-mail: i.tagliaro@campus.unimib.it;moncho@ugr.es

Abstract

Biocomposites of sepiolite clays and natural rubber latex represent novel green synthetic materials that provide improved mechanical performances following an ecofridenly and sustainable mixing procedure, without the use of surfactants. In this work, experiments and theory are combined to investigate the stability of colloidal dispersions formed by likely-charged sepiolite fibers and non-adsorbing natural rubber latex. For this purpose, a density functional approach was applied to calculate the depletion interaction between two sepiolite fibers induced by the presence of naturally charged natural rubber, and an effective one-component mean-field free energy was developed to predict the phase behavior of the colloid. The existence of a depletion attraction, enhanced by the electrostatic repulsion beweeen sepiolite and rubber latex, is shown to be strong

enough to induce the phase separation (flocculation) of the colloidal dispersion only at determined volume fractions. The theoretical predicted phase diagram is in excellent qualitative and quantitative agreement with the experimental results, indicating that this electrostatically-enhanced depletion effect plays a key role in the colloidal stability of this system. To the best of our knowledge, this study represents the first attempt to tackle how depletion effects, in terms of the depletion forces, can be exploited to produce sepiolite/natural rubber biocomposites.

Introduction

Elastomeric nanocomposites made of clay nanoparticles and natural rubber (NR) have been widely studied in the reinforcement of rubber matrices for tyre applications,[1,2] but are also relevant for the improvement of a number of other aspects such as barrier properties, electrical, membrane properties, polymer blend compatibility, and flammability resistance.[3]

Among the different methods to compound clay-NR nanocomposites,[4] latex compounding (LC) is known to be a simple, eco-friendly and effective procedure to obtain high dispersion and distribution of the clay filler, which are crucial aspects to achieve good mechanical performances of the composite material.[5]

LC consists in the mixing a polymer latex (synthetic polymers[6] or NR latex NRL[7]) with an aqueous dispersion of hydrophilic filler (i.e. montmorillonite,[8] paligroskite,[9] bentonite,[10] kaolinite[11]). The absence of organic solvents, the possibility of using natural available raw materials and the reduction of dust release provided by the aqueous dispersion, make LC a valuable compounding procedure in line with the environmental friendly EU policies.[12]

LC is particularly suitable for the compounding of clay minerals, whose efficient dispersion is still a challenge.[13] Among clays, sepiolite ($Si_{12}O_{30}Mg_8(OH,\ F)_4(H_2O)_{48}H_2O$) (Sep) is a natural phyllosilicate made of particles of high aspect ratio (AR $\sim$ 20) with fibers of micrometric length and nanometric width.[14,15] Its particles are arranged in structures of aggregates that prevent a good dispersion by simple mixing with the rubber matrix and,

therefore, require the use of a chemical modification to obtain high reinforcement.[16]

In a previous paper,[17]high loaded Sep/NR nanocomposites were produced by applying LC without the use of any flocculating agents, usually required for the coagulation process. These materials showed excellent mechanical properties in comparison with nanocomposites obtained with traditional melt mixing. This has been related to the efficacy of the LC distribution,[18] obtained through the break down of the filler aggregates in water.

In ordinary LC techniques,[19] flocculation is usually driven by the addition of a flocculating agents (i.e. acids or inorganic salts), molecules able to destabilize the system and trigger a phase separation of the solid particles from the solvent.

In detail, flocculating agents act against the stability of aqueous dispersion, controlled by the surface charge of the particles, which results in the Derjaguin, Landau, Verwey, Overbeek (DLVO)-type electric double layer repulsion.[20] For industrial processes, the suppression of the stabilizing effect provided by the charge is usually achieved through the addition of electrolytes,[21] but this approach has several disadvantages and may end in undesired effects on the material properties such as oxidation of the polymer or alteration of the vulcanization efficiency .[22]

Alternatively, another method to induce destabilization of aqueous dispersions is the use of polymeric flocculants. In this case, the presence of the polymer determines the phase separation thanks mainly to two mechanisms of interaction with the solid particle dispersion: adsorption of polymers (bridging flocculation) or non-adsorption of polymers (depletion flocculation).[21]

Bridging flocculation occurs when a polymer is adsorbed onto more than one particle, thus causing particle attraction. Adsorbing polymers have been exploited for different applications including water treatment, coating and cement formulations, and paper manufacturing.[23]

On the other hand, depletion flocculation has been described as an effect of destabilization driven by osmotic forces, which are generated in colloidal dispersions due to geometrical aspects of the particles.[24,25] These polymer-induced phase separation mechanisms have been

studied and quantified through calculations and mathematical theories.[26] Almost all existing work on depletion flocculation has been focused on theoretical calculation of the phase behavior of such systems.[21,27] Moreover, the theoretical-experimental studies are few when applied to rod-sphere systems.[28] Thus, we identified a lack in the literature of industrial applications of depletion flocculants with regards to the production of clay/polymer nanocomposites. To our knowledge, there are no examples of how depletion flocculation can be exploited to make sepiolite/NR nanocomposites.

In this work, phase separation experiments were performed by mixing dispersions of Sep and NRL at different volume fractions. These experimental data were compared to a density functional theory (DFT) calculation, taking into account the entropic and electrostatic depletion forces involved in the destabilization of such colloidal dispersion. It was shown that the electrostatic repulsion between likely-charged sepiolite and NRL particles gives rise to a significant enhancement of the depletion attraction between Sep particles. This effect, which has been already observed in mixtures of charged spherical colloids[29] and charged colloid-polymer mixtures,[30,31] is able to induce the phase separation of the system even for relatively small concentration of NRL polymers. In addition, through a theoretical quantification of the depletion forces, it is shown how the variation of the volume fraction of Sep or NRL particles may be applied to the compounding of nanocomposite through LC procedures.

The present study may be relevant in highlighting how electrostatically-enhanced depletion forces can be exploited to induce phase separation in aqueous dispersions by the use of non-adsorbing polymers for industrial applications. Moreover, this work may help in the definition of the particle morphological aspects and of the volume fraction limits within which depletion forces are generated.

After explaining the experimental setup and the characterization of the materials,the applied theoretical model is described. The theory explains the calculation of all the direct interactions, of the depletion potential with and without the electrostatic effect (exploiting the concepts of DFT under some approximations) and allows the definition of the colloidal

dispersion phase diagram. Finally, the theoretical predictions are compared to the experimental observations.

Experimental setup and materials

Materials and Methoods

Sepiolite Pangel S9 (Sep) was supplied by Tolsa and extracted from the landfill of Vallecas (Spain) and NRL Medium Ammonia (MA), (60% w/w) and poly(1,4-cis-isoprene) STR20 by Von Bundit (Von Bundit CO., Phuket, Thailand). Milli-Q water with a resistivity 18.2 MW cm was utilized. HCl (37% w/w) and NH_4OH (28–30% w/w) were purchased from Sigma-Aldrich. Dynamic light scattering (DLS) and ζ-potential were analyzed by Malvern Zetasizer Nano Series ZS90 instrument (Malvern Panalytical Ltd., Malvern, UK) to assess the hydrodynamic diameter of NRL particles and the particle charges of both NRL and Sep. For the DLS and ζ-potential analyses, the NRL sample was diluted approximately 1:1 and Sep dispersed at a dilution of 0.1 gL-1, in both cases making use of Milli-Q water. The ζ-potential measurement on Sep and NRL were performed at 25 °C at different pH by adding a suitable amount of HCl or NH_4OH solution to NRL and Sep dispersion in order to check the isoelectric point and the stability of the dispersions in the vicinity of the working pH. Scanning Electron Microscopy (SEM) analysis was performed by a Vega TS5136 XM Tescan microscope (Tescan Brno s.r.o., Kohoutovice, Czech Republic) to characterize the Sep particle dimensions, with 30 kV electron beam excitation, 25 pA beam current, 12 mm of working distance and beam spot of 38 nm. Samples were gold-sputtered, prior to SEM analysis. The particle dimensions were measured manually with ImageJ processing program (Image Processing and Analysis in Java, Version No 2, National Institutes of Health, Bethesda, MD, USA). The evaluation of the Sep length and diameter were calculated as average of the dimensions of 100 fibers in 20 different (SEM) micrographs. Transmission Electron Microscopy (TEM) Zeiss EM 900 microscope (Zeiss, Oberkochen, Germany) operating at 80 kV was used to characterize NRL

particles. One drop of NRL diluted 1:100 was deposited on the TEM grid, left to dry in the air and analyzed.

Experiments on the flocculation of Sep/NRL system

Different amounts of Sep were dispersed in water (400 mL) with a mechanic stirrer (Velp Scientifica, Usmate (MB), Italy) at 200 rpm (right per minute) for 60 min, sonicated for 10 min and mixed again for 10 min. In another vessel, different amount of NRL were diluted with 100 mL of distilled water and stirred for 10 min at 100 rpm with a mechanic stirrer. Then, the previous Sep dispersion was poured into the diluted NRL solution, under stirring at 500 rpm. Experimental observations of the flocculation were made on the base of the visible separation of a solid phase from the solvent. In Table 1, it is reported the set of experiments thought in order to observe the flocculation of the Sep-NRL system.

Arturo can you insert Table 1 for me? Or otherwise give me suggestions on how to do it because it seems very much compicated

Characterization of Sep and NRL

characterization.pdf

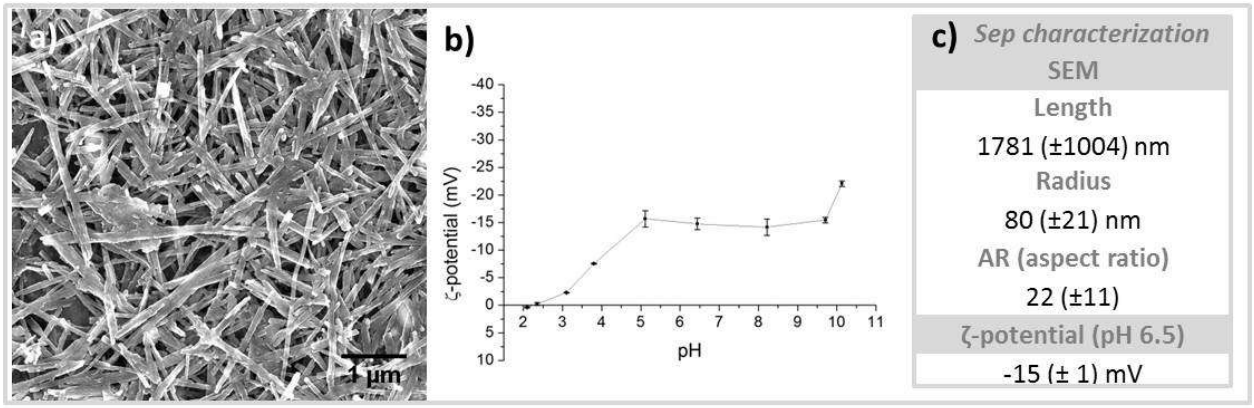

Figure 1: Characterization of Sep: a) SEM; b) ζ-potential; c) summary of parameters used in the DFT calculation.

From the SEM in Figure 1(a), Sep particles appear as rod like objects with high anisotropy.

As reported in Figure 1(c), the measured length and width of particles are respectively 1781 (± 1004) nm and 80 (± 21) nm. The particle size is very polydispersed especially in length as reported in literature .[32] The Sep particles are structurally constituted by a chessboard architecture of alternating tunnel-like cavities which extend throughout the fiber direction. The fibers are sometimes interconnected in bundles-like aggregates which may reach the dimension of hundreds of micrometers. The statistical analysis performed on the SEM picture has been used to model the rods dimension for the calculations. The stability of the Sep dispersion was evaluated by ζ-potential (Figure 1 b). Around the pH of 6.5 (naturally reached by the dispersion of Sep particles) the dispersion reaches the ζ-potential values of -15 mV. The negative charge of Sep is determined by the ionization of hydroxyle groups which are present on the particle surface.[33] Varing the pH, the system reaches the values of -24 mV (high pH) and +1 mV (low pH), defining the isoelectric point around 2.4, as reported in literature.[34]

characterization.pdf

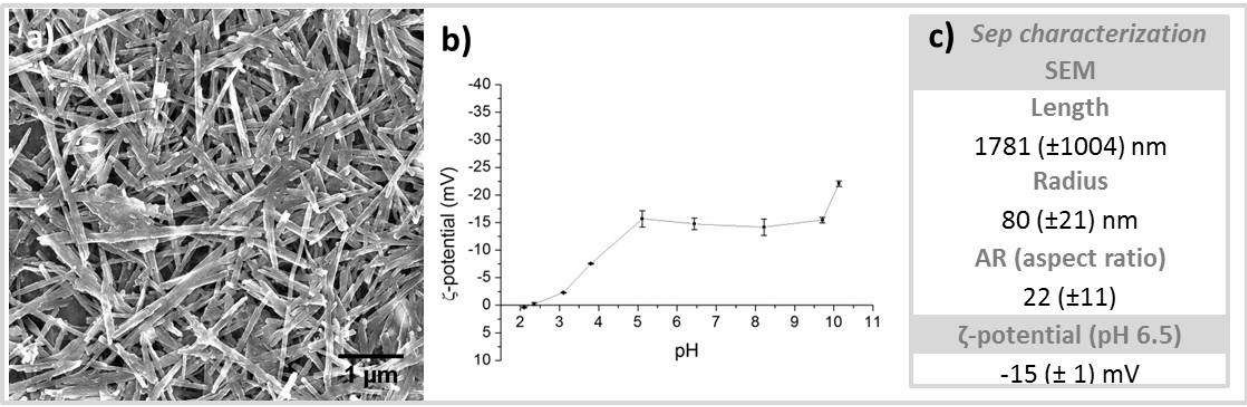

Figure 2: Characterization of NRL: a) SEM; b) summary of parameters used in the DFT calculation; c) DLS; d) ζ-potential.

The characterization of NRL particle dimension was assessed by DLS and confirmed by TEM analysis (Figure 2a and c). NRL particles are difficult to image since they are very soft and tend to form a film when dried on solid supports, thus, TEM analysis was made to check the DLS results. DLS analysis (Figure 2c) of diluted NRL shows a bimodal distribution of the hydrodynamic radius, indicating the presence of particles with an average size of 270

nm (around 60%), and a second population of 1200 nm (around 40%). This result is in line with the literature which reports very polydispersed systems .[35] Moreover, the TEM image (Figure 2a) confirms the DLS analysis showing spherical objects of variable diameter ranging from 1500 nm to 200 nm. NRL ζ-potential was characterized over a wide pH range. This assessment was made in order to evaluate the isoelectric point and the variation of stability in the vicinity of the pH at which the experiments were performed. At pH 8, ζ-potential of diluted NRL is -28 mV. Going to low pH, the system defines a isoelectric point of 2.9, in agreement with the literature.[36] NRL particles are known to be surrounded by proteins and phospholipids which expose amino and carboxyl functional groups that are ionized in water and responsible of the negative charge detected by ζ-potential.[35] In Table 1 the parameters taken from Sep and NRL characterization useful for the DFT calculation are summarized.

Table 1: Main characteristics of the cylindrical sepiolite and spherical NRL particles used in the experiments: length (L), radius (R_c, R_p), zeta potantial (ζ), charge (Z_c, Z_p) and volume fraction (ϕ_c, ϕ_p).

Header one	L (nm)	R_c (R_p) (nm)	ζ (mV)	Z_c (Z_p)	ϕ_c (ϕ_p)
Sepiolite	1780	40	-15	-7584	0.01538
NRL	-	175	-28	-505137	≤ 0.06

The total volume fractions of Sep cylinders and NR polymer spheres were calculated assessing the volume of one particle with the characteristics of length and radius reported in Table 1. Since Sep and NRL are both negatively charged at the working pH (pH of the Sep/NRL colloidal dispersion= 7), they repell each other. In this way, NRL do not adsorb onto the Sep surface (non-adsorbing polymer), effect which guarantees that the concentration of NRL particles is very small close to the Sep particles.

Theoretical framework

The system under study is a binary colloidal dispersion of Sep and NRL. NRL has been modelled as inter-penetrable spherical charged polymer, whereas Sep particles has been treated as

hard (impenetrable) charged cylinders (see Figure 3). Both sepiolite and NRL are immersed in an aqueous electrolyte solution with monovalent salt NH_4OH, at a fixed concentration of 5.714 mM. The solvent (water) has been considered as a continuum background with a constant dielectric permittivity ϵ_r. In addition, the ions of the suspension are not explicitly considered. Instead, coarse-grain simplification has been applied and it has been assumed that the electrostatic interactions between cylinders and polymers are given by the corresponding screened effective potentials for the given salt concentration.

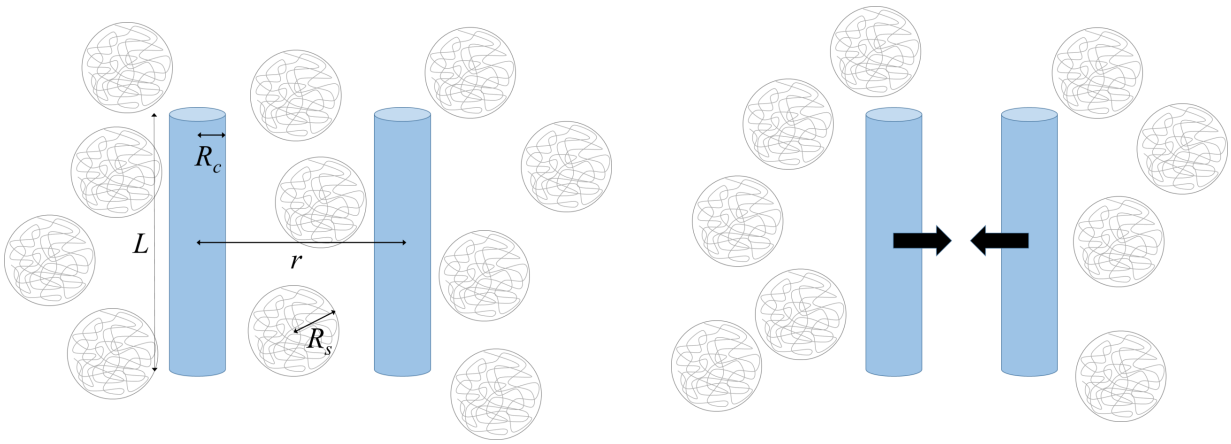

Figure 3: Illustration of the excluded-volume depletion effect between two Sep cylinders. One Sep particle is represented by a blue cylinder and one NRL particles by a shpere, where L=lenght, r=distance between two Sep particles, R_C=radius of the cylinder, R_S=radius of the shepre)

Henceforth, subindexes c and p will design the Sep cylinders and the NRL shperes, respectively. Analogously, $V_{cc}(r)$, $V_{cp}(r)$ and $V_{pp}(r)$ will represent the Sep-Sep, Sep-NRL and NRL-NRL pair interaction potentials. L will denote the length of the cylinder, R_c its radius, and R_p the radius of the NRL polymer. The volume fraction of Sep cylinders and NRL spheres are given $\phi_c = \pi R_c^2 L \rho_c^{bulk}$ and $\phi_p = 4\pi R_p^3 \rho_p^{bulk}/3$, where ρ_c^{bulk} and ρ_p^{bulk} are the number densities of both components in the bulk solution.

The first goal of our theory is the determination of the effective interaction potential between a pair of Sep cylinders induced by the presence of the spherical NRL shperes, $V_{cc}^{eff}(r)$. For this purpose, theoretical model based on DFT was developed to calculate the depletion interaction potential between Sep cylinders. It was assumed that both cylinders are

orientated in parallel, as this orientation maximizes the effect of the depletion interaction (see Figure 3). This effective interaction can be split into two contributions, namely the direct screened electrostatic repulsion, plus the depletion potential induced by the charged NRL (Eq. 1).

$$V_{cc}^{eff}(r) = V_{cc}(r) + V_{cc}^{dep}(r) \tag{1}$$

The second goal of this work is to provide a theoretical explanation of the phase behavior of the Sep and NRL colloidal dispersion. For this purpose, $V_{cc}^{eff}(r)$ is used to construct a one-component mean-field free-energy to predict the phase behavior and identify the stable and unstable regions of the phase diagram and the location of the critical point.

Particle interactions

First of all, we start calculating the pair interaction potentials involved in the system. Ions coming from the monovalent salt distribute around the cylinders forming the so-called ionic double layer. In order to find analytical expressions of these potentials, Sep cylinders were assumed to be very long compared to the spherical polymer, so to consider Sep particles as rods of infinite length and neglect border effects. It was also assumed that the electrostatic potential can be deduced from the linearized Poisson-Boltzmann equation for weakly charged particles, in the so-called Debye-Hückel approximation.

With this two approximations, the pair interaction potential between two sepiolite particles with bare charge Z_c is given by Eq. 2 (full demostration given in Appendix):

$$\beta V_{cc}(r) = \begin{cases} \infty & r \leq 2R_c \\ \frac{2l_B Z_c^2}{L} \left(\frac{1}{\kappa R_c \mathrm{K}_1(\kappa R_c)} \right)^2 \mathrm{K}_0(\kappa r) & r > 2R_c. \end{cases} \tag{2}$$

where $l_B = e^2/(4\pi\epsilon_0\epsilon_r k_B T)$ is the Bjerrum length, κ is the inverse Debye screening length, defined as $\kappa = \sqrt{8\pi l_B \rho_s}$ (ρ_s is the salt concentration), and where $\mathrm{K}_0(x)$ and $\mathrm{K}_1(x)$ are the zeroth and first order Bessel function of the second kind, respectively. Please note that Eq. 2

may be generalized to highly charged particles replacing the bare charge by the effective charge Z_c^{eff}.

Following the same procedure, the pair interaction between a Sep cylinder and a charged NRL sphere (Eq. 3) may be expressed as

$$\beta V_{cp}(r) = \begin{cases} \infty & r \leq R_{cp} \\ Z_p^{eff} e\psi(r) & r > R_{cp}. \end{cases} \tag{3}$$

where $R_{cp} = R_c + R_p$ and $\psi(r)$ is the electrostatic potential induced by a charged Sep cylinder at a distance r (see Eq. 27 of the Appendix). Due to the counterion penetration inside the soft NRL polymer, its effective charge Z_p^{eff} is related to the bare charge Z_p (Eq. 4) .[37,38]

$$Z_p^{eff} = \frac{3Z_p}{\kappa^2 R_p^2}\left[\cosh(\kappa R_p) - \frac{\sinh(\kappa R_p)}{\kappa R_p}\right] \tag{4}$$

Therefore Eq. 5 follows.

$$\beta V_{cp}(r) = \begin{cases} \infty & r \leq R_{cp} \\ 6Z_c Z_p \frac{l_B}{L} \frac{\cosh(\kappa R_p) - \sinh(\kappa R_p)/(\kappa R_p)}{\kappa^3 R_p^2 E_c \mathrm{K}_1(\kappa R_c)} \mathrm{K}_0(\kappa r) & r > R_{cp}. \end{cases} \tag{5}$$

Finally, the interaction between two charged NR polymer shperes $V_{pp}(r)$ can be obtained modelling them as soft spherical particles with a more or less uniform distribution of charge. Since a polymer globule is not a hard sphere, ions can penetrate inside, reducing drastically its effective charge, as predicted by Eq. 4. Given the small concentration of NR polymer and the large salt concentration (of the order of 10 mM) employed in the experiments, the electrostatic interaction between two NRL particles is weak and short-ranged. Therefore, as a first approximation this interaction was neglected and $V_{pp} \approx 0$ was considered as it only represents a small perturbation compared to the other contributions, namely V_{cc} and V_{cp}.

Free energy functional for the Sep-NRL colloidal dispersion

Given the small volume fractions of Sep and NRL used in the experiments ($\phi_c = 0.0154$ and $\phi_p < 0.06$) and the fact that the salt concentration is high enough to provide a significant screening of the electrostatic interactions, an analytical expression for the two-component free energy in the low-density limit is defined in Eq. 6,

$$\beta F_{ex}\left[\rho_c, \rho_p\right] = -\frac{1}{2}\sum_{i.j=c,p}\int\int d\vec{r}d\vec{r}\,'\rho_i(\vec{r})\rho_j(\vec{r}')f_{ij}(\vec{r}-\vec{r}\,') \tag{6}$$

where $\beta = 1/(k_BT)$ (k_B is the Boltzmann constant and T the absolute temperature), $\rho_i(\vec{r})$ ($i = c, p$) are the number density of both components at position $\vec{r}$, and $f_{ij} = exp(-\beta V_{ij}) - 1$ is the so-called Mayer function between particles i and j. The depletion interaction between Sep cylinders can be obtained following the *test particle route*.[39,40] With this method, a Sep particle is fixed at the origin $\vec{r} = 0$ and makes an external potential for the colloidal dispersion. Due to this external potential, the rest of Sep and NRL develop a non-uniform density profile around the central particle. Then, a second Sep cylinder is inserted into the inhomogeneous mixture at distance r from the first particle. Using this procedure, the depletion potential between Sep particles in the infinite dilution limit ($\rho_c \to 0$) is given by

$$\beta V_{cc}^{dep}(\vec{r}) = c_c^{(1)}(\infty) - c_c^{(1)}(\vec{r}) \tag{7}$$

where $c_c^{(1)}(\vec{r})$ is the one-body correlation function, defined as the functional derivative of the excess free energy

$$c_c^{(1)}(\vec{r}) = -\beta\frac{\delta F_{ex}[\rho_c, \rho_p]}{\delta\rho_c(\vec{r})} \tag{8}$$

Using Eq. 6 and 8 into Eq. 7 we find

$$\beta V_{cc}^{dep}(\vec{r}) = -\int d\vec{r}\,'(\rho_p(\vec{r}\,') - \rho_p^{bulk})f_{cp}(\vec{r}-\vec{r}\,') \tag{9}$$

A more simple approximation can be written neglecting the interaction between NRL particles. This assumption can be safely done if the Sep-NRL interaction dominates over the NRL-NRL interaction or if the number density of NRL is small. Under this approximation, the density profile of NRL particles around a single Sep can be expressed by the distribution of an ideal gas

$$\rho_p(\vec{r}) \approx \rho_p^{bulk} e^{-\beta V_{cp}(\vec{r})}, \tag{10}$$

so

$$\beta V_{cc}^{dep}(\vec{r}) = -\frac{\rho_p^{bulk}}{1-\phi_c} \int d\vec{r}\,' f_{cp}(\vec{r}\,') f_{cp}(\vec{r}-\vec{r}\,') \tag{11}$$

11 provides the depletion potential between a pair of Sep particles separated by a distance r, induced by the presence of charged NR polymer shperes. Please note the polymer number density has been normalized as $\rho_p^{bulk}/(1-\phi_c)$ to take into account the real available volume left by the Sep particles in the system. An explicit expression to perform this integral is given in Eq. 42 of the Appendix.

In the special case of neutral NR polymer spheres, the depletion potential is exclusively caused by volume exclusion effects. Indeed, since NRL particles can not occupy the space around Sep, a depletion layer of radius $R_{cp} = R_c + R_p$ emerges around the cylinders. If the distance between two Sep particles is smaller than $2R_{cp}$, the overlap between the depletion regions around both cylinders gives rise to an increase of the total available volume for the NRL particles, which implies an increase of entropy. We will refer to this effect as *entropic depletion*. In this particular situation, the Mayer function is given by the Heaviside step function $f_{cp}(r) = -\theta(R_{cs} - r)$, so

$$\beta V_{cc}^{dep,ent}(\vec{r}) = -\frac{\rho_p^{bulk}}{1-\phi_c} \int d\vec{r}\,' \theta(R_{cs} - r\,')\theta(R_{cs} - |\vec{r}-\vec{r}\,'|) \tag{12}$$

The calculation of this volume integral can be performed analytically, leading to the following

expression for the entropic depletion attraction (details of this calculation in Appendix)

$$\beta V_{cc}^{dep,ent}(r) = \begin{cases} -\frac{\rho_p^{bulk}}{1-\phi_c} L \left[2R_{cp}^2 \arccos(\frac{r}{2R_{cp}}) - \frac{r}{2}\sqrt{4R_{cp}^2 - r^2} \right] & r \leq 2R_{cp} \\ 0 & r > 2R_{cp}, \end{cases} \tag{13}$$

where r is again the distance between the longitudinal axes of two parallel Sep cylinders.

One-component effective free energy and phase diagram

In this paragraph, a good estimate of the free energy was found to determine the phase diagram of the colloidal dispersion. There are multiple ways to perform this task. The more complete model would be to consider a full two-component free energy, valid also for concentrated suspensions. In our model, instead, the free energy given in Eq. 6 can only be applied in the dilute regime conditions.

However, another possibility is to use the depletion interaction obtained in the previous paragraph in the so-called effective one-component framework. In this method, the system is considered to be formed exclusively by Sep particles that interact among them through the effective potential $V_{cc}^{eff}(r) = V_{cc}(r) + V_{cc}^{dep}(r)$, where V_{cc} is given by Eq. 2, and V_{cc}^{dep} obtained through Eq. 11. In other words,our effective depletion potential was extended for any volume fraction. This technique has been successfully applied to investigate the phase diagram and the interfacial behavior of neutral colloid-polymer mixtures.[41,42]

Figure 4 clearly shows that the direct pair interaction between two Sep particles, $V_{cc}(r)$, obtained using Eq. 2 with the experimental values of L, R_c and Z_c provided in Table 1 is very abrupt at short distance. Consequently, this interaction can safely approximated by an effective hard rod with a new effective hard rod diameter larger than the original diameter, $\sigma_c' > \sigma_c$. In fact, the effective diameter can be calculated matching the second virial coefficient of the rod-rod electrostatic repulsion, $V_{cc}(r)$, with the corresponding value

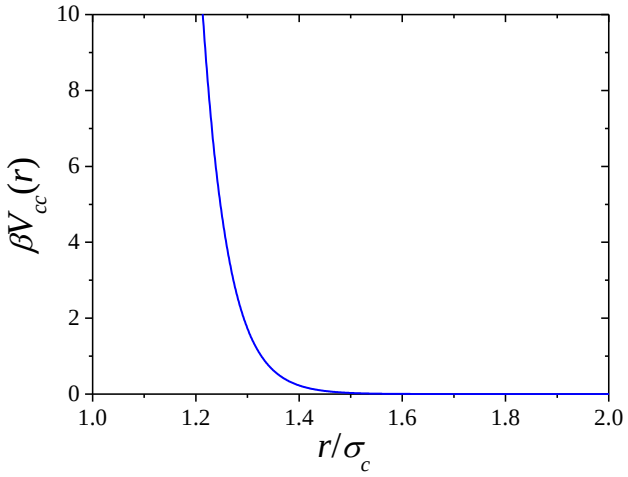

Figure 4: Direct pair potential between two parallel Sep particles as a function of the distance between their longitudinal axes ($V_{cc}(r)$), for particles with $L = 1789$ nm. $\sigma_c = 2R_c = 80$ nm and $Z_c = -7584$, immersed in a NH_4OH aqueous solution at $\rho_s = 5.714$ mM and $T = 298$ K.

for an uncharged hard rod.

$$B_2 = -\pi L \int_0^\infty \left[e^{-\beta V_{cc}(r)}\right] r dr \equiv B_2^{HR} = \frac{1}{2}\pi L(\sigma_c^{eff})^2 \tag{14}$$

where $\sigma_c' = 2R_c'$ is the effective diameter of the cylindrical particles. After some algebra, Eq. 14 leads to the following expression, where the integral is now performed in the dimensionless separation $z = r/\sigma_c$

$$\sigma_c' = \sigma_c\sqrt{1-2q} \quad q = \int_1^\infty \left[e^{-\beta V_{cc}(z)} - 1\right] z dz \tag{15}$$

Using the pair potential $V_{cc}(r)$ shown in Figure 4, $q = -0.4207$ was obtained, meaning that $\sigma_c' = 1.357\sigma_c$. The real Sep volume fraction and the effective one are related by $\phi_c' \approx 1.841\phi_c$.

In our model, the effective one-component is split into three additive contributions

$$\frac{F}{V} \equiv f = f_{ideal} + f_{HR} + f_{dep} \tag{16}$$

The first term is the ideal contribution, given by

$$\beta f_{ideal} = \rho_c \left[\ln(\rho_c \Lambda_c^3) - 1\right] \tag{17}$$

The second term represents the hard rod free energy density. For this contribution, we make use of the analytical expression provided by Hentschke *et al.* obtained using scaled particle theory for a nematic fluid of parallel hard spherocylinders[43]

$$\beta f_{HR} = \left[-\ln(1-\phi_c') + \frac{3\phi_c'}{1-\phi_c'} + b_3 \left(\frac{\phi_c'}{1-\phi_c'}\right)^2\right] \rho_c \tag{18}$$

where

$$b_3 = \frac{3}{2}\frac{1 + 3L/\sigma_c' + 2(L/\sigma_c')^2}{\left(1 + 3L/(2\sigma_c')\right)^2} \tag{19}$$

Finally, the third contribution in Eq. 16 represents the free energy induced by the depletion attraction effect. Since the depletion attraction is weak (due to the small concentration of NRL used in the experiments) and long-ranged (due to the large size of the NR polymer shperes compared to the Sep particles), a mean-field form is been assumed for this term

$$\beta f_{dep} = \frac{1}{2}\rho_c^2 \int \beta V_{cc}^{dep}(r) d\vec{r} \tag{20}$$

f_{dep} is negative due to the attractive character of the depletion interaction, and it is the responsible of the phase separation. In fact, if the depletion attraction is intense, then the free energy density develops a convex region between two concave regions, which leads to a gas-liquid phase separation (gas and liquid denote a fluid dilute and dense phases of Sep particles). Conversely, if the depletion attraction is not strong enough, the free energy density becomes a concave function of the Sep density and the system is always stable. The coexistence phases can be obtained making use of the common tangent construction. Basically, it consists in finding out the Sep concentrations with the same chemical potential

and the same pressure, i.e. $\mu_c(\rho_{c,gas} = \mu_c(\rho_{c,liq})$ and $P_c(\rho_{c,gas} = P_c(\rho_{c,liq})$, where

$$\mu_c = \left(\frac{\partial f}{\partial \rho_c}\right)_T \qquad P_c = -f + \rho_c \left(\frac{\partial f}{\partial \rho_c}\right)_T \tag{21}$$

Results and discussion

The previously explained theoretical model was applied to the Sep and NRL colloidal dispersion described in the experimental Section. This mixture is a water based dispersion at temperature $T = 298$ K, with a relative permitivity $\epsilon_r = 78.39$, and a salt concentration $\rho_s = 5.714$ mM. Values of particle size, length and ζ potential for both species are shown in Table1. At these conditions, the inverse Debye screening length is $\kappa^{-1} = 4.02$ nm, which is very small compared to the size of both particles. This confirms that the tails of the electrostatic interactions are short-ranged. The bare charge of the Sep particles have been obtained assuming that the electrostatic potential at the particle surface is $\psi_0 \approx \zeta$ and making use of Eq. 28. This leads to $Z_c = -7584$.

The calculation of the charge of the NRL shperes is more complex because these particles are soft particles that allow the permeation of ions and water molecules at distances $r < R_p$. The penetration of solvent inside the particles increases the value of the electrophoretic mobility (μ_e) compared to the mobility of a hard colloid of the same bare charge and size. On the other hand, the counterion penetration strongly reduces the effective charge of the particle, decreasing the electrophoretic mobility. The measured mobility of these particles, $\mu_e = -2.14 \cdot 10^{-8}$ $\mathrm{m^2V^{-1}s^{-1}}$, is the combination of these effects. Among the analytical theories that describe all these effects, Ohshima[44] deduces several analytical expressions for soft particle electrophoretic mobility in terms of two parameters, κ and λ. The first is the inverse Debye screening length and the second characterizes the internal friction exerted by the solvent on the NR polymer spheres (in fact, λ^{-1} provides an estimate of the solvent penetration distance inside the NRL internal volume). In our case $\kappa R_p = 43.5 \gg 1$, and

λR_p is larger that κR_p. In this limit, μ_e is given by

$$\mu_e = \frac{1}{\eta_s \kappa^2} \frac{Z_p e}{4\pi R_p^3} \tag{22}$$

which leads to a NRL charge of $Z_p = -505137$.

Effective Sep-Sep pair potential

Appling the theory, the effective pair potential between two Sep cylinders ($V_{cc}^{eff}(r)$) has been calculated in two different situations. In the first case, NRL are assumed to be uncharged, so the depletion attraction induced by the NRL particles is only caused by excluded volume effects. Basically, when two Sep cylinders approach each other until a distance smaller than $r < 2(R_c + R_p)$, there is not enough space to fit any NRL particle in the region between the cylinders. Therefore, the NRL particles generates a force from outside the excluded space, creating an unbalanced osmotic pressure that exerts an effective depletion attraction between the Sep particles. This case can be regarded as a reference situation to compare with, and will be denoted as *entropic depletion*. Expression 13 provides the analytical formula for this depletion pair potential.

In the second case, the NRL particles are charged, so the depletion attraction is enhanced by the electrostatic interaction. Indeed, the electrostatic repulsion between likely-charged Sep and NRL paricles reinforces the volume exclusion effect, which induces a stronger and longer-range effective attraction compared to the entropic depletion. This case will be refered as *electrostatic depletion*. The new range of the depletion potential depends on the salt concentration. For low electrolyte concentration, the electric double layers around both cylinders are extended, and so the electrostatic depletion has a very long range. For high salt concentration, on contrary, the electrostatic depletion only leads to a small increase of the range of the attraction compared to the entropic effect. In our experimental conditions, the concentration of monovalent salt is 5.714 mM so the screening length in the system is

about 4 nm, which is quite small compared to the size of the NRL. Therefore, we do not expect a significant increase of the attraction range of the electrostatic depletion compared to the entropic one. The calculation of $V_{cc}^{dep}(r)$ is obtained from the numerical integration of Eq. 11.

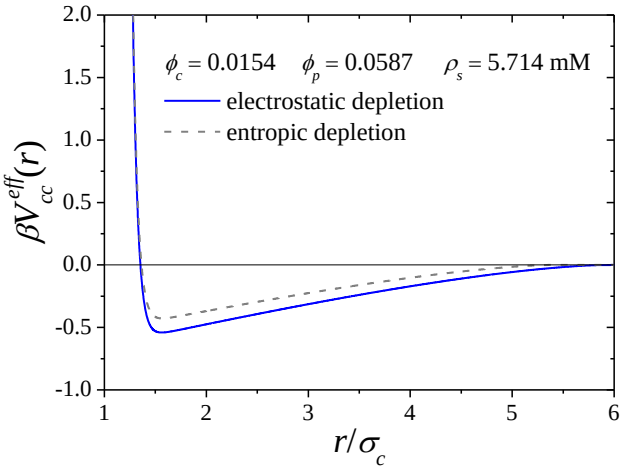

Figure 5: Effective pair potential between two parallel Sep particles induced by uncharged and charged NR polymer spheres (entropic and electristatic depletion, respectively) as a function of the distance between their longitudinal axes ($V_{cc}^{eff}(r)$) obtained for Sep and NRL volume fractions given by $\phi_c = 0.0154$ and $\phi_p = 0.0587$, respectively. In both cases $\rho_s = 5.714$ mM ant $T = 298$ K.

Figure 5 shows the effective pair potential obtained for Sep and NRL volume fractions of $\phi_c = 0.0154$ and $\phi_p = 0.0587$, considering the entropic and the electrostatic depletion (dashed gray and blue lines respectively). As observed, both effective pair interactions show a sharp short-range repulsive barrier caused by the strong electrostatic repulsion between Sep particles at small distances ($r \lesssim 1.36\sigma_c$). At longer distance, the depletion of NR polymer spheres around the Sep cylinders develops an attractive potential well located at $r \approx 1.5\sigma_c$. However, the electrostatic depletion leads to a deeper attractive potential compared to the entropic depletion induced by purely excluded-volume effects. The range of the attraction is also larger due to the longer range of the electrostatic depletion. For the entropic depletion, the range of the attraction is given by $2R_{cp} = \sigma_c + 2R_p = 5.375\sigma_c$. In fact, the range of the electrostatic depletion attraction enlarges the range of about $0.1\sigma_c = 8$ nm, which is totally consistent with the electrostatic interaction range of $2\kappa^{-1} = 8.04$ nm.

Phase behavior

These results clearly indicate that the exclusion of the charged NR polymer spheres, due to the combination of excluded-volume and electrostatic repulsion, induces a considerable amount of attraction between the charged Sep rods. Therefore, the question is whether this attraction is strong enough to provoke the phase separation of the system, i.e. flocculation. So, it is necessary to define the phase diagram of the colloidal dispersion, or at least the binodal for gas-liquid phase separation. In this context, gas and liquid refer to diluted and concentrated phases of Sep particles, respectively. If the depletion attraction is strong enough to situate the colloidal dispersion in the unstable region, phase separation will occur and a dense liquid phase will be formed, leading to the flocculation of the system. If the system is located in the stable region, it will remain as a stable and homogenous dispersion.

In order to obtain the phase diagram, the effective depletion interaction calculated in the previous section has been inserted in the one-component free energy model shown in the theoretical framework of this paper. This free energy includes the ideal contribution, the hard rod contribution, and the mean-field depletion term (see Eqs. 16-20). The location of the liquid-gas coexistence curve has been obtained solving numerically Eqs. 21 using the common-tangent construction. This procedure has been applied for both cases, namely entropic depletion and electrostatic depletion. The resulting $\phi_c - \phi_p$ liquid-gas coexistence line are shown in Figures 6(a) and (b) as dashed gray (entropic depletion) and solid blue lines (electrostatic depletion). The critical points are denoted as circles at the bottom of the binodal line. Both plots depict the same results, with the only difference that the bottom graph uses logarithm scale to expand the low-ϕ_c region.

The discussion firstly takes into account the diagram obtained considering electrostatic depletion. Below the critical point ($\phi_c^{crit} = 0.17$,$\phi_p^{crit} = 0.038$) the depletion attraction is too weak to induce phase separation, so both components are gently mixed without phase-separating forming a stable and homogeneous fluid. In the region located on the left of the coexistence line, the system forms a stable diluted gas of Sep particles, whereas on the

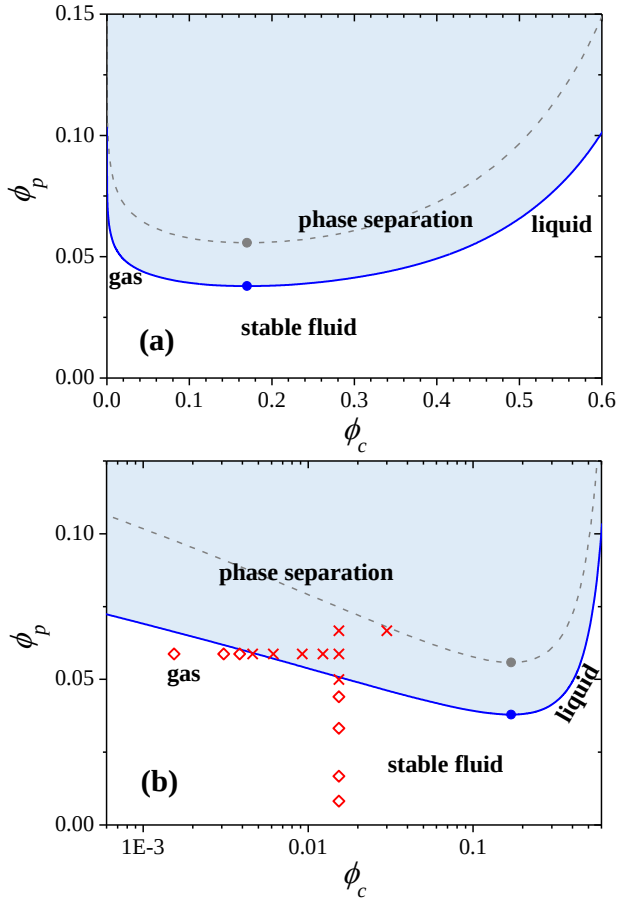

Figure 6: $\phi_c - \phi_p$ liquid-gas coexistence line predicted by our theoretical model considering electrostatic depletion (blue solid line) and entropic depletion (gray dashed line), for $\rho_s = 5.714$ mM ant $T = 298$ K. Blue and gray circles represent the corresponding critical points of the binodals. Red diamonds and red crosses denote the experimentally measured points of the diagram that lead to a stable or unstable (flocculating) systems, respectively.

right it forms a condensed fluid, where the volume fraction Sep particles is very high. If the colloidal dispersion is above the critical point and above the coexistence line (shadow region), it becomes unstable: a dispersion prepared inside this region will eventually phase separate into a Sep diluted (gas) and concentrated (liquid) phases. The coexistence line identify the onset of flocculation. For a fixed value of ϕ_p the blue line provides the concentration of both phases. The tie lines that connect both phases through the unstable region are horizontal (not shown). In fact, strictly speaking ϕ_p represents the NRL volume fraction in the reservoir, i.e. a system free of Sep coupled in equilibrium with the original mixture.

If the coexistence line is calculated using entropic depletion (gray dashed line), it is clearly

appreciable that the resulting binodal shifts to higher NRL volume fractions. The reason of this effect is to refer to the shape of the depletion attraction (Figure 5). Since entropic depletion leads to a less intense and shorter effective attraction, the NRL volume fraction must be further increased to achieve phase separation, thus shifting the critical point and the whole coexistence line to larger values of ϕ_p.

The experimental data are represented by red symbols in Figure 6(b). Red diamonds represent stable Sep-NRL colloidal dispersions, whereas red crosses correspond to unstable dispersions that undergo flocculation. As observed, the coexistence line predicted by the effective one-component model provides a qualitative and quantitaive explanation of the experimental results. These data point out that, in order to induce flocculation, increasing the NRL packing fraction above the critical is not always enough, as it is also needed to increase the Sep concentration for entering the unstable region of the diagram.

It is very important to emphasize here that the electrostatic enhancement of the depletion attraction is required to justify the experimental results. For instance, if we try to explain these results using only the entropic (purely excluded-volume) depletion, what we find is that the binodal is well above both experimental data, so both experimental points should be stable. Therefore, models simply based on entropic depletion can not explain the stability of charged colloidal dispersions.

Conclusions

This work aimed at assessing the possibility of exploiting electrostatic depletion forces generated in colloidal dispersions to produce biocomposites for industrial applications. DFT calculations were made on the base of Sep and NRL particle characterization and were compared to experiments on the flocculation of Sep/NRL colloidal dispersions. The DFT results show the existence of a depletion attraction which is enhanced by the electrostatic repulsion generated between likely-charged Sep and NR polymer particles. The calculated phase di-

agram is in excellent qualitative and quantitative agreement with the experimental results, indicating that electrostatically-enhanced depletion are determinant in the colloidal stability of this system. The exclusion of the charged NR polymer spheres, due to the combination of excluded-volume and electrostatic repulsion, induces a considerable amount of attraction between the charged Sep rods, thus determining the macroscopic effect of flocculation. The phase diagram calculated by DFT highlights that the generation of electrostatic depletion forces may be exploited to produce Sep/NR biocomposites in working conditions above the critical point of volume fractions $\phi_c^{crit} = 0.17$,$\phi_p^{crit} = 0.038$. In this case, the depletion attraction is strong enough to induce phase separation (flocculation) of the colloidal dispersion. On the other hand, the same dispersion below the critical point remains in a stable suspension. Moreover, the definition of the coexistence line that identifies the onset of flocculation evidences the necessity to work in conditions where particles are charged since otherwise the purely entropic depletion is not strong enough to create forces able to trigger flocculation. This work wants to give a quantified physical explanation for the macroscopic behavior of colloidal dispersions that are relevant in industrial application such as LC. We expect that this work will help in the development of sustainable synthetic strategies to produce nanocomposites made of charged anisotropic particles and non-adsorbing polymers without the need of any synthetic flocculating agents, taking advantage of electrostatic depletion forces generated in colloidal dispersions.

Acknowledgement

A. M-J. the financial support provided by the Spanish "Ministerio de Economía y Competitividad (MINECO), Plan Nacional de Investigación, Desarrollo e Innovación Tecnológica (I + D + i)" (Project FIS2016-80087-C2-1-P) and the European Regional Development Fund (ERDF).

Appendix

Electrostatic potential around a single charged cylindrical colloid immersed in monovalent salt solution

In this first Section of the Appendix we will deduce the expression of the electrostatic potential ψ around a single charged cylinder immersed in a 1:1 electrolyte suspension in the Debye-Hückel approximation. Since we are assuming very long cylinders ($L > R_c$), ψ depends only of the distance to the central axe. Making use of the Poisson equation

$$\nabla\psi(r) = \frac{1}{r}\frac{d}{dr}\left(r\frac{d\psi}{dr}\right) = -\frac{\rho_e(r)}{\epsilon_0\epsilon_r} \qquad r > R_c, \tag{23}$$

where $\rho_e(r)$ is the local charge density of counterions and coions around the cylinder, which we assume to follow the Boltzmann equation

$$\rho_e(r) = e\left[\rho_+(r) - \rho_-(r)\right] = -2e\rho_s \sinh(\beta e\psi(r)) \tag{24}$$

Inserting Eq. 24 into 23 and taking the limit of small electrostatic potentials, we obtain the linearized Poisson-Boltzmann equation

$$\frac{1}{r}\frac{d}{dr}\left(r\frac{d\psi}{dr}\right) = \kappa^2\psi(r) \tag{25}$$

where $\kappa^2 = 2e^2\rho_s/(\epsilon_0\epsilon_r k_B T)$. The general solution to this differential equation that fulfills the condition $\psi(r \to \infty) = 0$ is

$$\psi(r) = A\mathrm{K}_0(\kappa r) \qquad r > R_c \tag{26}$$

where K_0 is the zeroth order Bessel function of the second kind. Far away from the cylindrical particle K_0 decays asymptotically as $\mathrm{K}_0(x) \sim \sqrt{\pi/2}\exp(-x)/\sqrt{x}$. Imposing electroneutral-

ity ($\psi'(R_c)2\pi R_c L = Z_c e/(\epsilon_0\epsilon_r)$) leads to the final solution

$$\psi(r) = \frac{Z_c e}{2\pi\epsilon_0\epsilon_r L}\frac{1}{\kappa R_c \mathrm{K}_1(\kappa R_c)}\mathrm{K}_0(\kappa r) \qquad r > R_c \tag{27}$$

where K_1 is the first order Bessel function of the second kind. The relation between Z_c and the surface potential ψ_0 (defined as $\psi(r) = \psi_0 \mathrm{K}_0(\kappa r)/\mathrm{K}_0(\kappa R_c)$) is given by

$$Z_c = \frac{2\pi\epsilon_0\epsilon_r L}{e}\frac{\kappa R_c \mathrm{K}_1(\kappa R_c)}{\mathrm{K}_0(\kappa R_c)}\psi_0 \tag{28}$$

Calculation of the electrostatic interaction between two hard charged cylinders in parallel orientation

The electrostatic force between two parallel cylinders immersed in 1:1 electrolyte solution may be obtained integrating the electrostatic Maxwell tensor, defined as

$$\hat{\mathrm{T}} = \left(\Delta\Pi + \frac{1}{2}\epsilon_0\epsilon_r E^2\right)\hat{\mathrm{I}} - \epsilon_0\epsilon_r \vec{E}\vec{E} \tag{29}$$

where $\hat{\mathrm{I}}$ is the identity tensor, E is the electrostatic field, and $\Delta\Pi$ is the osmotic pressure induced by the ions. Assuming that ions can be treated as an ideal gas and using the Boltzmann distribution, the osmotic pressure can be written as

$$\Delta\Pi(r') = k_B T\left[\rho_+(r') + \rho_-(r') - 2\rho_s\right] = 2k_B T\rho_s\left[\cosh(\beta e\psi(r')) - 1\right] \tag{30}$$

In the limit of low electrostatic potentials, the osmotic pressure can be expanded up to second order in ψ. This leads to

$$\Delta\Pi(r') \approx k_B T\rho_s\beta^2\phi^2(r') = \frac{1}{2}\epsilon_0\epsilon_r\kappa^2\psi^2(r') \tag{31}$$

Tensor $\hat{T}$ has to be integrated on the median perpendicular plane separating both cylin-

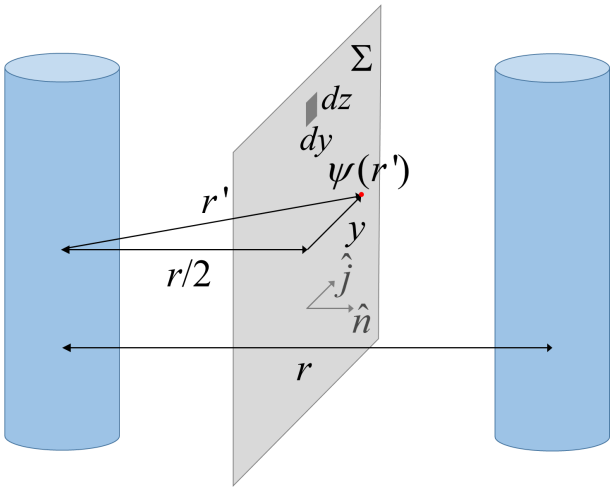

Figure 7: Schematic representation of the middle plane between two parallel cylinders and the variables used in the integration to calculate the force between two charged cylinders.

ders to calculate the electrostatic force between both cylinders[45] (see Figure 7)

$$\vec{f} = \int\int_{\Sigma} \hat{\mathrm{T}} \cdot d\vec{S} = \epsilon_0 \epsilon_r \int\int_{\Sigma} \left[\frac{1}{2} \left(\kappa^2 \psi^2 + E^2 \right) \hat{n} - (\vec{E} \cdot \hat{n}) \vec{E} \right] dS \tag{32}$$

where $\hat{n}$ is the unit vector perpendicular to the median plane, $dS = dydz$. Since both cylinders are assumed to be infinitely long, ψ and $\vec{E}$ do not depend on coordinate z, and the z component of the electric field is zero, so $\vec{E} = E_x \hat{n} + E_y \hat{\jmath}$. In addition, the integration over the term with component $\hat{\jmath}$ is also zero due to symmetry considerations. Hence,

$$\vec{f} = \frac{1}{2} \epsilon_0 \epsilon_r L \int_{\infty}^{\infty} \left[\kappa^2 \psi^2 - E_x^2 + E_y^2 \right] dy \hat{n} = \epsilon_0 \epsilon_r L \int_{0}^{\infty} \left[\kappa^2 \psi^2 - E_x^2 + E_y^2 \right] dy \hat{n} \tag{33}$$

In the context of the Debye-Hückel approximation, the total electrostatic potential can be obtained adding the unperturbed electrostatic potentials generated by both cylinders:

$$\psi(r') = \psi^{(1)}(r') + \psi^{(2)}(r') = 2A\mathrm{K}_0(\kappa r') \tag{34}$$

The electrostatic field is $\vec{E} = -d\psi(r')/dr\hat{r}'$ so

$$E_x = 0 \qquad E_y = 2A\kappa \mathrm{K}_1(\kappa r')\frac{y}{r'} \tag{35}$$

Using Eqs. 34 and 35 into 33 leads to

$$\vec{f} = 4\epsilon_0\epsilon_r L A^2\kappa^2 \int_0^\infty \left[\mathrm{K}_0^2(\kappa r') + \mathrm{K}_1^2(\kappa r')\frac{y^2}{r'^2}\right] dy\hat{n} \tag{36}$$

This integral is analytically solvable substituting $y = \sqrt{r'^2 - r^2/4}$ and integrating over $r' \in [r/2, \infty]$. The solution is

$$\vec{f} = 2\pi\epsilon_0\epsilon_r L A^2\kappa \mathrm{K}_1(\kappa r)\hat{n} \tag{37}$$

The electrostatic interaction pair potential between both cylinders is the integral of the electrostatic force

$$V_{cc}(r) = -\int_r^\infty f = 2\pi\epsilon_0\epsilon_r L A^2 \mathrm{K}_1(\kappa r) \tag{38}$$

Using Eqs. 26 and 27 to express A in terms of the cylinder charge, Z_c, finally leads to

$$V_{cc}(r) = \frac{Z_c^2 e^2}{2\pi\epsilon_0\epsilon_r L}\left(\frac{1}{\kappa R_c \mathrm{K}_1(\kappa R_c)}\right)^2 \mathrm{K}_0(\kappa r). \tag{39}$$

Calculation of the depletion attraction between sepiolite particles induced by non-adsorbing NRL polymers

Using Eq. 5 for the sepiolite-NRL interaction, the Mayer function can be written as

$$\beta f_{cp}(r) = \begin{cases} -1 & r \leq R_{cp} \\ e^{-C\mathrm{K}_0(\kappa r)} & r > R_{cp}. \end{cases} \tag{40}$$

where C is a dimensionless constant given by

$$C = 6Z_c Z_p \frac{l_B}{L} \frac{\cosh(\kappa R_p) - \sinh(\kappa R_p)/(\kappa R_p)}{\kappa^3 R_p^2 E_c \mathrm{K}_1(\kappa R_c)} \tag{41}$$

Due to the cylindrical symmetry, the volume integral implied in Eq. 11 can be written as a two-dimensional surface integral expressed in polar coordinates $dS = r_1 dr_1 d\theta_1$ (see Figure 8)

$$\begin{aligned} \beta V_c c^{dep}(r) = -\frac{\rho_p^{bulk}}{1-\phi_c} L \int_0^{\infty} \int_0^{2\pi} f_{cp}(r_1) f_{cp}(r_2) r_1 dr_1 d\theta_1 = \\ -\frac{\rho_p^{bulk}}{1-\phi_c} L \int_0^{\infty} r_1 f_{cp}(r_1) dr_1 \int_0^{2\pi} f_{cp}(\sqrt{r^2 + r_1^2 - 2 r r_1 \cos\theta_1}) d\theta_1 \end{aligned} \tag{42}$$

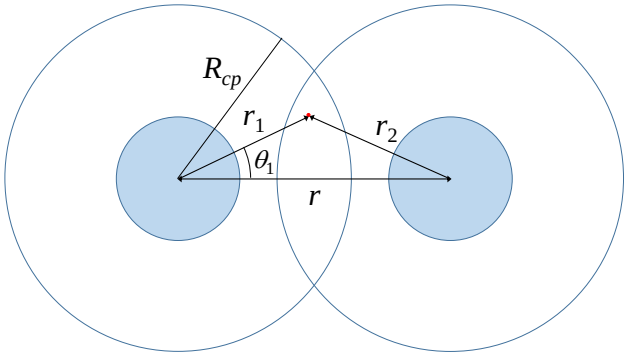

Figure 8: Illustration of the variables used to calculate the surface integral given in Eq. 42.

In general, this double integral has to be performed numerically. However, for neutral NRL polymers it can be solved analytically. In this case the Mayer functions is $f_{cp}(r) = -\theta(R_{cp} - r)$ and the depletion effects becomes purely entropic. It is a very simple task to show that the integrand of Eq. 42 is zero in every point of the space, with the exception of the overlapping region between two intersecting circles of radius R_{cp} separated by a center-to-center distance of r. Hence

$$\beta V_{cc}^{dep,ent} = -\frac{\rho_p^{bulk}}{1-\phi_c} L S_{overlap}(r; R_{cp}) \tag{43}$$

where $S_{overlap}$ is the overlapping surface between the circles of radius R_{cp}, given by

$$S_{overlap}(r; R_{cp}) = \begin{cases} 2R_{cp}^2 \arccos(r/(2R_{cp})) - (r/2)\sqrt{4R_{cp}^2 - r^2} & r \leq 2R_{cp} \\ 0 & r > 2R_{cp}. \end{cases} \quad (44)$$

References

(1) Di Credico, B.; Cobani, E.; Callone, E.; Conzatti, L.; Cristofori, D.; D'Arienzo, M.; Dirè, S.; Giannini, L.; Hanel, T.; Scotti, R. Size-controlled self-assembly of anisotropic sepiolite fibers in rubber nanocomposites. *Applied Clay Science* **2018**, *152*, 51–64.

(2) Cobani, E.; Tagliaro, I.; Geppi, M.; Giannini, L.; Leclère, P.; Martini, F.; Nguyen, T. C.; Lazzaroni, R.; Scotti, R.; Tadiello, L.; Di Credico, B. Hybrid Interface in Sepiolite Rubber Nanocomposites: Role of Self-Assembled Nanostructure in Controlling Dissipative Phenomena. *Nanomaterials* **2019**, *9*, 486.

(3) Kanny, K.; Mohan, T. In *Progress in Rubber Nanocomposites*; Thomas, S., Maria, H. J., Eds.; Woodhead Publishing Series in Composites Science and Engineering; Woodhead Publishing, 2017; pp 153 – 177.

(4) Karger-Kocsis, J.; G. Gatos, K. *Rubber Nanocomposites: Preparation, Properties and Application*; 2010; pp 169–195.

(5) Kotal, M.; Bhowmick, A. K. Polymer nanocomposites from modified clays: Recent advances and challenges. *Progress in Polymer Science* **2015**, *51*, 127 – 187, Environmentally Relevant and Hybrid Polymer Materials.

(6) Gui, Y.; Zheng, J.; Ye, X.; Han, D.; Xi, M.; Zhang, L. Preparation and performance of silica/SBR masterbatches with high silica loading by latex compounding method. *Composites Part B: Engineering* **2016**, *85*, 130 – 139.

(7) Saravari, O.; Boonmahitthisud, A.; Satitnaithum, W.; Chuayjuljit, S. Mechanical and

Electrical Properties of Natural Rubber/Carbon Nanotube Nanocomposites Prepared by Latex Compounding. Environmental and Materials Engineering. 2013; pp 543–546.

(8) Valadares, L.; Leite, C.; Galembeck, F. Preparation of natural rubber–montmorillonite nanocomposite in aqueous medium: evidence for polymer–platelet adhesion. *Polymer* **2006**, *47*, 672 – 678.

(9) Othman, N.; Muttalib, S. N. A.; Ismail, N. I. The Effect of Surface Modification on the Properties of Palygorskite Filled Natural Rubber Nanocomposite. *Macromol. Symp.* **2019**, *371*, 35–43.

(10) Varghese, S.; Karger-Kocsis, J. Natural rubber-based nanocomposites by latex compounding with layered silicates. *Polymer* **2003**, *44*, 4921 – 4927.

(11) Ruamcharoen, J.; Chotisuwan, S.; Ruamcharoen, P. Tensile Properties and Morphology of Natural Rubber-Kaolinite Organoclay Composites. Key Engineering Materials II. 2012; pp 701–705.

(12) Lightsey, J.; Kneiling, D.; Long, J. Silica wet masterbatch: A new process for predispersion of silica in emulsion polymers. *Rubber World* **1998**, *218*, 35–40.

(13) Rooj, S.; Das, A.; Stöckelhuber, K. W.; Heinrich, G. *Clay Reinforcement in Natural Rubber on Micro and Nano Length Scales*; 2013; pp 220–246.

(14) Wilson, I. Applied Clay Mineralogy. Occurrences, processing and application of kaolins, bentonite, palygorskitesepiolite, and common clays. *Clays and Clay Minerals* **2007**, *55*, 644–645.

(15) Murray, H. H. In *Applied Clay Mineralogy*; Murray, H. H., Ed.; Developments in Clay Science; Elsevier, 2006; Vol. 2; pp 141 – 145.

(16) Credico, B. D.; Cobani, E.; Callone, E.; Conzatti, L.; Cristofori, D.; D'Arienzo, M.; Dirè, S.; Giannini, L.; Hanel, T.; Scotti, R.; Stagnaro, P.; Tadiello, L.; Morazzoni, F.

Size-controlled self-assembly of anisotropic sepiolite fibers in rubber nanocomposites. *Applied Clay Science* **2018**, *152*, 51 – 64.

(17) Di Credico, B.; Tagliaro, I.; Cobani, E.; Conzatti, L.; D'Arienzo, M.; Giannini, L.; Mascotto, S.; Scotti, R.; Stagnaro, P.; Tadiello, L. A Green Approach for Preparing High-Loaded Sepiolite/Polymer Biocomposites. *Nanomaterials* **2019**, *9*, 46.

(18) Tadiello, L.; Cipolletti, V. R.; Giannini, L.; Hanel, T.; Galimberti, M.; Scotti, R.; Di Credico, B.; Morazzoni, F.; D'Arienzo, M.; Tagliaro, I. Elastomeric Compositions Comprising Silicate Fibres With Needle-Shaped Morphology Of Nanometric Size And Tyres For Vehicles That Comprise Them. 2018.

(19) Adachi, Y. Dynamic aspects of coagulation and flocculation. *Advances in Colloid and Interface Science* **1995**, *56*, 1 – 31.

(20) Quemada, D.; Berli, C. Energy of interaction in colloids and its implications in rheological modeling. *Advances in Colloid and Interface Science* **2002**, *98*, 51 – 85.

(21) de Yan, Y.; Burns, J. L.; Jameson, G. J.; Biggs, S. The structure and strength of depletion force induced particle aggregates. *Chemical Engineering Journal* **2000**, *80*, 23 – 30.

(22) Joseph, R. *Practical Guide to Latex Technology*; Smithers Rapra, 2013.

(23) Benn, F.; Fawell, P.; Halewood, J.; Austin, P.; Costine, A.; Jones, W.; Francis, N.; Druett, D.; Lester, D. Sedimentation and consolidation of different density aggregates formed by polymer-bridging flocculation. *Chemical Engineering Science* **2018**, *184*, 111 – 125.

(24) Asakura, S.; Oosawa, F. On Interaction between Two Bodies Immersed in a Solution of Macromolecules. *The Journal of Chemical Physics* **1954**, *22*, 1255–1256.

(25) Asakura, S.; Oosawa, F. Interaction between particles suspended in solutions of macromolecules. *J. Polym. Sci.* **1958**, *33*, 183–192.

(26) Myakonkaya, O.; Eastoe, J. Low energy methods of phase separation in colloidal dispersions and microemulsions. *Advances in Colloid and Interface Science* **2009**, *149*, 39 – 46.

(27) Vrij, A. Polymers at Interfaces and the Interactions in Colloidal Dispersions. 1976; `https://www.degruyter.com/view/j/pac.1976.48.issue-4/pac197648040471/pac197648040471.xml`.

(28) Park, C.-Y.; Fygenson, D. K.; Saleh, O. A. Electrostatics and depletion determine competition between 2D nematic and 3D bundled phases of rod-like DNA nanotubes. *Soft Matter* **2016**, *12*, 5089–5095.

(29) Ojeda-Mendoza, G. J.; Moncho-Jordá, A.; González-Mozuelos, P.; Haro-Pérez, C.; Rojas-Ochoa, L. F. Evidence of electrostatic-enhanced depletion attraction in the structural properties and phase behavior of binary charged colloidal suspensions. *Soft Matter* **2018**, *14*, 1355–1364.

(30) Peláez-Fernández, M.; Moncho-Jordá, A.; Callejas-Fernández, J. Structure of charged colloid-polymer mixtures. *EPL (Europhysics Letters)* **2010**, *90*, 46005.

(31) Peláez-Fernández, M.; Moncho-Jordá, A.; Callejas-Fernández, J. Charged colloid-polymer mixtures: A study on electrostatic depletion attraction. *The Journal of Chemical Physics* **2011**, *134*, 054905.

(32) Galan, E. Properties and applications of palygorskite-sepiolite clays. *Clay Minerals* **1996**, *31*, 443–453.

(33) Lu, F. J.; Hsu, S. L. A vibrational spectroscopic analysis of the structure of natural rubber. *Rubber chemistry and technology* **1987**, *60*, 647–658.

(34) Doğan, M.; Türkyilmaz, A.; Alkan, M.; Demirbaş, z. Adsorption of copper (II) ions onto sepiolite and electrokinetic properties. *Desalination* **2009**, *238*, 257–270.

(35) Sansatsadeekul, J.; Sakdapipanich, J.; Rojruthai, P. Characterization of associated proteins and phospholipids in natural rubber latex. *Journal of bioscience and bioengineering* **2011**, *111*, 628–634.

(36) de Oliveira Reis, G.; Menut, P.; Bonfils, F.; Vaysse, L.; Hemar, Y.; Sanchez, C. Acid-induced aggregation and gelation of natural rubber latex particles. *Colloids and Surfaces A: Physicochemical and Engineering Aspects* **2015**, *482*, 9–17.

(37) Denton, A. R. Counterion penetration and effective electrostatic interactions in solutions of polyelectrolyte stars and microgels. *Phys. Rev. E* **2003**, *67*, 011804.

(38) Ohshima, H.; Kondo, T. Electrostatic Double-Layer Interaction between Two Charged Ion-Penetrable Spheres: An Exactly Solvable Model. *Journal of Colloid and Interface Science* **1993**, *155*, 499 – 505.

(39) Roth, R.; Evans, R.; Dietrich, S. Depletion potential in hard-sphere mixtures: Theory and applications. *Phys. Rev. E* **2000**, *62*, 5360–5377.

(40) Roth, R.; Masahiro, K. Depletion potential between large spheres immersed in a multicomponent mixture of small spheres. *The Journal of Chemical Physics* **2006**, *125*, 084910.

(41) Dijkstra, M.; Brader, J. M.; Evans, R. Phase behaviour and structure of model colloid-polymer mixtures. *Journal of Physics: Condensed Matter* **1999**, *11*, 10079–10106.

(42) Moncho-Jordá, A.; Dzubiella, J.; Hansen, J. P.; Louis, A. A. Density-Functional Study of Interfacial Properties of Colloid-Polymer Mixtures. *J. Phys. Chem. B* **2005**, *109*, 6640–6649.

(43) Hentschke, R.; Taylor, M. P.; Herzfeld, J. Equation of state for parallel hard spherocylinders. *Phys. Rev. A* **1989**, *40*, 1678–1680.

(44) Ohshima, H. Electrophoresis of soft particles: Analytic approximations. *ELECTROPHORESIS* **2006**, *27*, 526–533.

(45) Bell, G.; Levine, S.; McCartney, L. Approximate methods of determining the double-layer free energy of interaction between two charged colloidal spheres. *Journal of Colloid and Interface Science* **1970**, *33*, 335 – 359.

Graphical TOC Entry